



Defence Research and
Development Canada

Recherche et développement
pour la défense Canada



Novel application of FTIR spectroscopy for the passive standoff detection of radiological materials

*E. Puckrin
J.-M. Thériault
H. Lavoie
D. Dubé
DRDC Valcartier*

Defence R&D Canada – Valcartier

Technical Memorandum

DRDC Valcartier TM 2004-365

August 2006

Canada

Novel application of FTIR spectroscopy for the passive standoff detection of radiological materials

E. Puckrin
J.-M. Thériault
H. Lavoie
D. Dubé
DRDC Valcartier

Defence R&D Canada – Valcartier

Technical Memorandum

DRDC Valcartier TM 2004-365

August 2006

Author

Eldon Puckrin

Approved by

Jean-Marc Garneau
Section Head, Space Optronics

Approved for release by

Gilles Bérubé
Chief Scientist

© Her Majesty the Queen as represented by the Minister of National Defence, 2006

© Sa majesté la reine, représentée par le ministre de la Défense nationale, 2006

Abstract

An investigation is made into the possibility of applying the long-wave passive standoff detection technique to the identification of radiological materials. This work is based on laboratory measurements of the diffuse reflectance from a number of radiological or related products, including UO_2 , UO_3 , U_3O_8 , CoO , Co_2O_3 , IrO_2 , ThO_2 , SrO , I_2O_5 , La_2O_3 , and yellow cake. The measured laboratory reflectance signatures were incorporated into the MODTRAN4 radiative transfer model to simulate the nadir radiances of various radiological compounds for three different sensor altitudes. The results of the simulations suggest that passive standoff radiometry may potentially detect and identify radiological materials. Further evidence to support the applicability of the method is based on measurement results from a field trial held at Defence Research and Development Canada – Valcartier involving the passive detection of SrO at standoff distances of 10–40 m.

Résumé

Ce mémorandum présente une étude des possibilités d'utilisation de la télédétection passive dans l'infrarouge lointain pour l'identification des produits radiologiques. Ce travail est basé sur des mesures en laboratoire de la réflectivité diffuse d'un certain nombre de produits radiologiques ou associés, tels que UO_2 , UO_3 , U_3O_8 , CoO , Co_2O_3 , IrO_2 , ThO_2 , SrO , I_2O_5 , La_2O_3 et le "yellow cake". Les signatures mesurées en laboratoire ont été incorporées au modèle de transfert radiatif, MODTRAN4, afin de simuler le rayonnement nadir de plusieurs composés radiologiques à trois altitudes différentes, soit 1 m, 1 km et 100 km. Les résultats des simulations suggèrent que la télédétection radiométrique passive peut potentiellement détecter et identifier les matériaux radiologiques. Des preuves additionnelles pour soutenir l'applicabilité de la méthode se basent sur les résultats de la télédétection du SrO à une distance de 40 m obtenue lors d'un essai qui a eu lieu au centre de Recherche et développement pour la défense Canada – Valcartier.

Executive summary

Passive standoff Fourier-transform infrared (FTIR) radiometry is a well-known technique for detecting and identifying chemical warfare agents. In addition to these potential threats, there is also the possibility of a release of radiological material by accident or terrorist activity. As a result it is important to have the necessary tools and techniques available for detecting and identifying radioactive products. At present, the main detection techniques depend on methods involving the measurement of a material's decay products.

The objective of this document is to determine if the passive standoff FTIR radiometric technique can also be used to detect and identify radiological products in outdoor environments. To accomplish this goal it was first necessary to determine if radiological materials have a signature in the thermal infrared region of the spectrum, where passive detection is possible. Through a series of diffuse reflectance measurements obtained in the laboratory, it is shown that a number of radiological materials, including several oxides of uranium (UO_2 , UO_3 , U_3O_8), the oxides of cobalt (CoO and Co_2O_3), iridium oxide (IrO_2), thorium oxide (ThO_2), strontium oxide (SrO), iodine oxide (I_2O_5) lanthanum oxide (La_2O_3) and yellow cake, have detailed infrared signatures that may make these compounds vulnerable to detection by passive radiometry.

The results of the laboratory reflectance measurements are followed by an investigation based on model simulations to determine the possibility of passively detecting and identifying radiological materials at the surface from a number of sensor altitudes. These simulations were performed using the MODTRAN4 radiative transfer model, which is able to characterize accurately at any altitude the thermal radiance that emanates from the atmosphere and from backgrounds having specific spectral reflectances. The simulated results indicate that there is potential for measuring radiological materials passively from several sensor altitudes. Finally, results from two passive radiometric measurements of SrO obtained in the field with the Compact Atmospheric Sounding Interferometer are presented for standoff distances of up to 40 m. These measurements support the conclusions determined from the simulation studies.

The development of a non-nuclear detection capability based on passive standoff FTIR radiometry may be a potentially effective addition to the existing arsenal of nuclear measurement techniques for the detection and identification of nuclear threats. Such a capability may also have an important application for the mining industry.

E. Puckrin, J.-M. Thériault, H. Lavoie and D. Dubé. 2006. Novel application of FTIR spectroscopy for the passive standoff detection of radiological materials, DRDC Valcartier TM 2004-365. Defence R&D Canada – Valcartier.

Sommaire

La télédétection passive par interférométrie infrarouge à transformée de Fourier (FTIR) est une technique acceptée pour la détection et l'identification d'agents chimiques militaires. En plus de ces menaces potentielles, il y a également la possibilité de dispersion de matériel radiologique provenant d'activités accidentelles ou terroristes. En conséquence, il est important d'avoir à notre disposition les outils et techniques nécessaires pour détecter et identifier les produits radiologiques. Les principales techniques de détection existantes dépendent de méthodes s'appuyant sur la mesure de la décroissance de la radioactivité des matériaux.

L'objectif de ce document est de déterminer si la technique de télédétection passive FTIR peut être employée pour détecter et identifier les produits radiologiques dans les environnements extérieurs. À cette fin, il était nécessaire de déterminer si les matériaux radiologiques ont une signature dans l'infrarouge thermique où la détection passive se produit. À l'aide d'une série de mesures de réflectivité diffuse obtenues en laboratoire, on montre qu'un certain nombre de matériaux radiologiques, c.-à-d. oxydes d'uranium (UO_2 , UO_3 , U_3O_8), oxydes de cobalt (CoO et Co_2O_3), l'oxyde d'iridium (IrO_2), l'oxyde de thorium (ThO_2), l'oxyde de strontium (SrO), l'oxyde de lanthane de l'oxyde d'iode (I_2O_5) (La_2O_3) et le "yellow cake", ont des signatures infrarouges détaillées qui peuvent rendre ces composés détectables par radiométrie passive.

Les résultats des mesures de réflectance diffuse en laboratoire sont suivis d'une étude de simulations avec des modèles pour déterminer la possibilité de télédétection passive et d'identification des matériaux radiologiques sur la surface terrestre pour un certain nombre d'altitudes. Ces simulations ont été effectuées en utilisant le modèle de transfert radiatif MODTRAN4, qui peut caractériser exactement le rayonnement thermique à n'importe quelle altitude qui émane de l'atmosphère et des milieux ayant des réflectivités spectrales déterminées. Les résultats simulés indiquent un certain potentiel à mesurer passivement les matériaux radiologiques pour des altitudes allant jusqu'à 100 kilomètres. Finalement, les résultats de deux mesures radiométriques passives de SrO obtenues à l'aide du spectromètre CATSI (Compact Atmospheric Sounding Interferometer) sont présentés pour des distances allant jusqu'à 40 m. Ces mesures viennent appuyer les conclusions de l'étude de simulation.

Le développement de techniques non nucléaires de détection basées sur la radiométrie passive FTIR peut être une addition potentiellement utile à l'arsenal des techniques de mesure qui existent déjà pour la détection et l'identification des menaces nucléaires. De telles possibilités peuvent également avoir une application importante sur l'industrie minière.

E. Puckrin, J.-M. Thériault, H. Lavoie and D. Dubé. 2006. Novel application of FTIR spectroscopy for the passive standoff detection of radiological materials, DRDC Valcartier TM 2004-365. Defence R&D Canada – Valcartier.

Table of contents

Abstract.....	i
Résumé	i
Executive summary	ii
Sommaire.....	iii
Table of contents	iv
List of figures	v
Acknowledgements	vii
1. Introduction	1
2. Detection Principles and Phenomenology	2
3. Measurement Approach.....	4
3.1 Laboratory measurements	4
3.2 Field measurements	5
4. Results and Analysis.....	7
4.1 Laboratory measurements of diffuse reflectance.....	7
4.2 Simulations of the passive standoff detection of radiological materials	8
4.2.1 Nadir radiance simulations of SrO	10
4.2.2 Nadir radiance simulations of UO ₂	11
4.2.3 Nadir radiance simulations of UO ₃	12
4.2.4 Nadir radiance simulations of yellow cake.....	13
4.3 Effect of temperature contrast on the passive standoff detection of radiological materials	15
4.4 Preliminary passive standoff measurements of radiological materials.....	16
5. Conclusions	18
6. References	19
Distribution list.....	21

List of figures

Figure 1: Diagram and parameters used to evaluate the radiance of a clean surface and a surface covered by a powdered contaminant.	3
Figure 2: Photographs of (A) Digilab FTS 3000 spectrometer and (B) DRIFTS accessory installed inside the sample compartment of the FTS 3000 for measuring the reflectance of radiological materials.	5
Figure 3: Schematic diagram of the optical arrangement used to measure reflectance spectra in the laboratory.	5
Figure 4: (A) Photograph and (B) optical diagram of the Compact ATmospheric Sounding Interferometer (CATSI) in the standard 10-cm telescope configuration used to passively detect and measure radiological compounds in the field.....	6
Figure 5: (A) Reflectance spectra measured by the DRIFTS technique for six radiological products over the 500–4000 cm^{-1} region. The measurements were obtained at a resolution of 4 cm^{-1} . (B) An expanded view of the reflectance spectra over the 700–1400 cm^{-1} (7–14 μm) thermal infrared region.....	7
Figure 6: (A) Reflectance spectra measured by the DRIFTS technique for five additional radiological products over the 500–4000 cm^{-1} region. The measurements were obtained at a resolution of 4 cm^{-1} . (B) An expanded view of the reflectance spectra over the 700–1400 cm^{-1} (7–14 μm) thermal infrared region.....	8
Figure 7: Transmission spectra for different optical depths of the atmosphere as simulated with the MODTRAN4 model.....	9
Figure 8: Contributions to total nadir radiance simulated for a sensor at an altitude of 1 km. 10	
Figure 9: (A) Direct total nadir radiance simulated for three sensor altitudes with a surface consisting of SrO. (B) Differential radiance simulated by subtracting the nadir radiance for a surface with a gray-body reflectance of 15% from the nadir radiance of a SrO surface.	11
Figure 10: (A) Direct total nadir radiance simulated for three sensor altitudes with a surface consisting of UO_2 . (B) Differential radiance simulation showing the nadir radiance for a concrete surface subtracted from the nadir radiance for a surface of UO_2 . The UO_2 absorption features are clearly visible in the differential spectra.	12
Figure 11: (A) Direct total nadir radiance simulated for three sensor altitudes with a surface consisting of UO_3 . (B) Differential radiance simulation showing the nadir radiance for a concrete surface subtracted from the nadir radiance for a surface of UO_3 . The UO_3 absorption features are clearly visible in the differential spectra.	13

- Figure 12: (A) Direct total nadir radiance simulated for three sensor altitudes with a surface consisting of yellow cake. (B) Differential radiance simulated by subtracting the nadir radiance with a gray-body surface reflectance of 1% from the nadir radiance with a yellow cake surface reflectance. The yellow cake absorption features are clearly visible in the differential spectra. 14
- Figure 13: Simulated effect of sky temperature on the passive detection of UO_3 . The sky temperature was altered by changing the base altitude of an optically thick cloud from 5 km to 250 m. (A) Direct total nadir radiance simulated for a surface consisting of UO_3 under varying cloud conditions. (B) Differential radiance simulated by subtracting the radiance of a blackbody at a surface temperature of 288.2 K from the radiance of a surface of UO_3 . The UO_3 absorption features diminish with increased sky temperature. 15
- Figure 14: (A) Photograph showing the powdered SrO sample sprinkled on the stone-tar surface. (B) CATSI spectrometer set up to measure the differential radiance of SrO at a standoff distance of 10 m. 16
- Figure 15: (A) Differential radiance spectra measured at a standoff distance of 10 m for a rooftop contaminated with SrO powder. The simulated differential spectrum of SrO is also presented for comparison. (B) Differential radiance spectra measured at a standoff distance of 40 m. 17

Acknowledgements

We would like to express our thanks to H el ene Gagnon and Eric Bergeron (DRDC Valcartier, Emerging Materials) for their help in obtaining the measurements of diffuse reflectance. We are also grateful to Philips Laou and Louis Durand (DRDC Valcartier, Microsystems) for fabricating the gold reference sample for the DRIFTS measurements.

This page intentionally left blank.

1. Introduction

Passive standoff detection by Fourier-transform infrared (FTIR) radiometry has become a relatively mature and reliable method for the identification and measurement of chemical warfare agents [1-5]. Recently, it has been shown to be a potentially valuable tool for identifying biological warfare agents as well [6,7]. Therefore, passive standoff detection based on FTIR radiometry plays a significant role in the detection and identification of chemical and biological (CB) hazards on the battlefield and as a counter-terrorism measure.

In addition to potential CB hazards, there is the possibility of a release of radiological material at a nuclear power plant or during the transportation of radioactive materials. An additional potential threat may originate from terrorist activity involving a radiological dispersion device (RDD), or dirty bomb, which could result in widespread radioactive contamination. As the result of a potential nuclear catastrophe, it is important to have the necessary tools and techniques for detecting and identifying radioactive products. At present, the main detection techniques depend on the measurement of particle emissions from the radioactively decaying material. This normally constitutes a measurement of the product's gamma rays or other emission particles including neutrons, and alpha and beta particles. The traditional means of detection depends largely on the strength of the emitting source. However, alpha and beta particle emissions are substantially attenuated by modest amounts of shielding, even by a sheet of paper in the case of alpha particles, which normally requires that the instrument be situated relatively close to the sources in order to detect their presence.

The objective of this paper is to determine if radiological products can be identified by a signature in the thermal infrared region (i.e., 8–14 μm), and to determine if such products can be detected and identified in outdoor environments by a passive sensor positioned at various distances from the material. The first part of this study concerns the laboratory measurements of diffuse reflectance for a number of radiological or related materials. The products considered in this study include the oxides of uranium (UO_2 , UO_3 , U_3O_8), the oxides of cobalt (CoO and Co_2O_3), iridium oxide (IrO_2), thorium oxide (ThO_2), strontium oxide (SrO), iodine oxide (I_2O_5), lanthanum oxide (La_2O_3), and yellow cake (a uranium ore). Of these materials, only the uranium and thorium compounds were radioactive. However, it is expected that the absorption spectra measured for non-radioactive isotopes will be similar to those of the radioactive counterparts; the small differences in mass will only result in a small shift in the spectral signature. The results of the laboratory reflectance measurements are followed by a study based on simulations with the MODTRAN4 transmission code [8]. A number of measurement scenarios involving various backgrounds and different sensor altitudes have been simulated to determine the possibility of passively detecting and identifying these radiological materials. Finally, results from passive measurements of SrO obtained in the field with the Compact Atmospheric Sounding Interferometer (CATSI) are presented for standoff distances of up to 40 m.

The development of a non-nuclear passive standoff detection capability based on FTIR radiometry may be a potentially effective addition to the existing arsenal of nuclear measurement techniques for the detection and identification of nuclear threats. This type of capability may also have an important application for the mining industry. This work was conducted under thrust 5E, Space Systems and Technology for Defence Applications.

2. Detection Principles and Phenomenology

A passive long-wave infrared standoff sensor functions by exploiting the temperature difference (ΔT) between the target scene and the background scene. If the target is warmer than the background, then the spectrum of the target chemical will be measured as an emission feature in the spectrum recorded by the sensor. Conversely, if the target is colder than the background, then the target chemical spectrum will be measured as an absorption feature. When a target consisting of a solid powder is present on a surface, ΔT is zero since the background (surface) and the powder are in contact. However, if the radiation from an external hot or cold source is reflected from the surface, then it is possible to observe the spectrum of the powder. In outdoor environments, the radiation from the cold sky provides a high surface-to-sky temperature difference that yields favourable detection possibilities. The radiative transfer associated with the detection of powdered targets is outlined below.

The radiative transfer intervening at a surface can be understood from a simple physical argument. A diagram is presented in Fig. 1 that defines the parameters used to evaluate the radiance emanating from a clean surface and from one contaminated with a powder; both are exposed to an outdoor environment. For a clean surface having a reflectance R_o , the spectral radiance measured at the sensor contains two components, i.e., the emitted radiance from the surface, $B(1 - R_o)$, and the cold sky radiance reflected by the surface, $L_{down} R_o$. The parameter L_{down} represents the downwelling radiance from the sky and B is the Planck radiance evaluated at the temperature (T) of the surface, which is given by

$$B = \left(\frac{1.191 \times 10^{-12} \nu^3}{e^{\left(\frac{1.439\nu}{T}\right)} - 1} \right), \quad (1)$$

where ν is the wavenumber in cm^{-1} and B is in $\text{W}/\text{cm}^2 \text{sr cm}^{-1}$. Adding these two radiance components, $B(1 - R_o)$ and $L_{down} R_o$, yields an expression for the radiance of the uncontaminated surface that is given by

$$L_{clean} = B - R_o(B - L_{down}). \quad (2)$$

Similarly, for a contaminated substrate consisting of a powder with a reflectance R_{cont} , as shown in Fig. 1, the spectral radiance measured by the sensor is given by

$$L_{cont} = B - R_{cont} (B - L_{down}). \quad (3)$$

A quantity of interest to study the radiative effects of a contaminant on a surface is the differential spectral radiance (ΔL), which is the radiance difference ($L_{cont} - L_{clean}$) obtained by subtracting Eq. (2) from Eq. (3),

$$L_{cont} - L_{clean} \equiv \Delta L = (R_o - R_{cont})(B - L_{down}). \quad (4)$$

Inspection of Eq. (4) reveals some simple facts concerning the sensitivity for detecting surface contaminants by passive spectral radiometry. First, the radiance difference is proportional to the reflectance contrast ($R_o - R_{cont}$), indicating that a highly reflecting surface results in an increased sensitivity for detection. Secondly, the radiance difference is proportional to the radiative contrast between the Planck surface radiance and the downwelling sky radiance, ($B - L_{down}$). Since the downwelling radiance increases with cloud cover, which in turn results in a decrease in the radiative contrast, the best detection possibilities are obtained for clear sky conditions where L_{down} is a minimum.

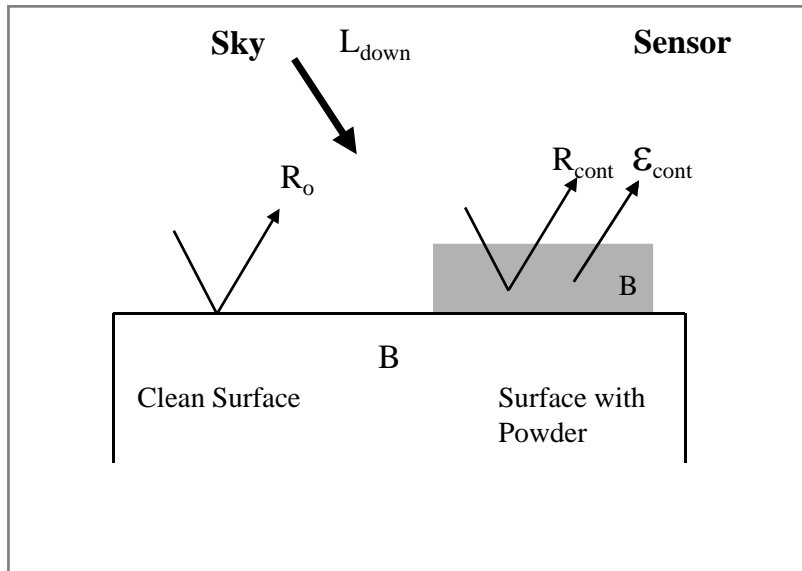


Figure 1: Diagram and parameters used to evaluate the radiance of a clean surface and a surface covered by a powdered contaminant.

3. Measurement Approach

3.1 Laboratory measurements

Diffuse reflectance infrared Fourier-transform spectroscopy (DRIFTS) is a simple method for acquiring reflectance spectra from powdered samples [9]. It was used in this work to measure the reflectance from powdered samples of UO_2 , UO_3 , U_3O_8 , CoO , Co_2O_3 , IrO_2 , ThO_2 , SrO , I_2O_5 , La_2O_3 , and yellow cake. The uranium samples were supplied by Cameco Corporation and all other products were purchased from Sigma-Aldrich, with purities exceeding 99% in all cases. The spectra were recorded with a Digilab Fourier-transform spectrometer (FTS 3000) equipped with a silicon carbide globar, Peltier-cooled DTGS detector and a Ge-coated KBr beamsplitter. The spectrometer was capable of a maximum resolution of 0.1 cm^{-1} ; however, in this work the measurements were recorded at a resolution of 4 cm^{-1} . Several spectra that were measured at a better resolution indicated that no additional spectral information was evident at the higher setting. Photographs of the Digilab FTS 3000 and the DRIFTS accessory installed within the sample compartment of the system are shown in Figs. 2A and 2B, respectively.

The diffuse reflectance apparatus (Spectra-tech, Inc.) consisted of a biconical optical arrangement, as illustrated in the schematic diagram in Fig. 3. Infrared radiation from the ceramic source was directed from the interferometer towards the parabolic mirror, M3, and focused on the sample cup filled with powder. The reflected diffuse radiation from the powdered sample was collected by another parabolic mirror, M5, and redirected towards the DTGS detector of the FTS system. The spot size illuminated by the infrared beam at the sample surface was less than 2 mm in diameter. A small piece of 600-grit silicon carbide paper with adhesive backing and coated with a $0.25\text{-}\mu\text{m}$ layer of pure gold by vapour deposition constituted the reference sample. Its absolute reflectance has been measured to be close to unity throughout the thermal infrared region [9].

The procedure for performing the reflectance measurements was as follows. The gold reference sample was first placed in the DRIFTS receptacle. The system was purged for 15 min to reduce the residual water vapour and carbon dioxide in the sample compartment of the spectrometer, and then a spectrum of the intensity of the radiation reflected from the gold surface was measured. The gold sample was then removed, and the receptacle was filled with one of the powdered radiological samples. After another 15-min purge, a spectrum of the radiation reflected from the powder was measured. The gold sample was replaced a second time and a measurement was obtained to confirm that the DRIFTS assembly gave reproducible results. The reflectance spectrum of the powder was determined from the ratio of the reflected intensities from the powder sample and gold sample.

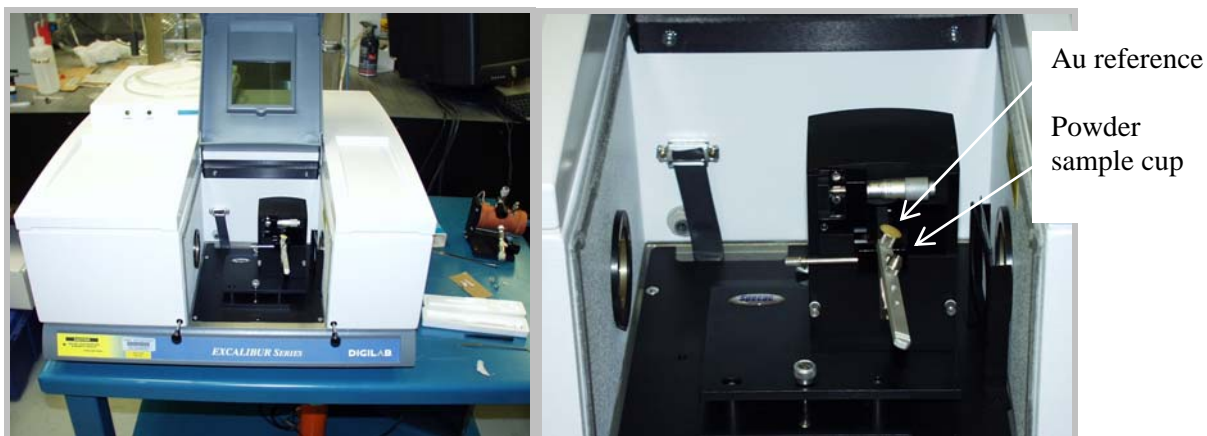


Figure 2: Photographs of (A) Digilab FTS 3000 spectrometer and (B) DRIFTS accessory installed inside the sample compartment of the FTS 3000 for measuring the reflectance of radiological materials.

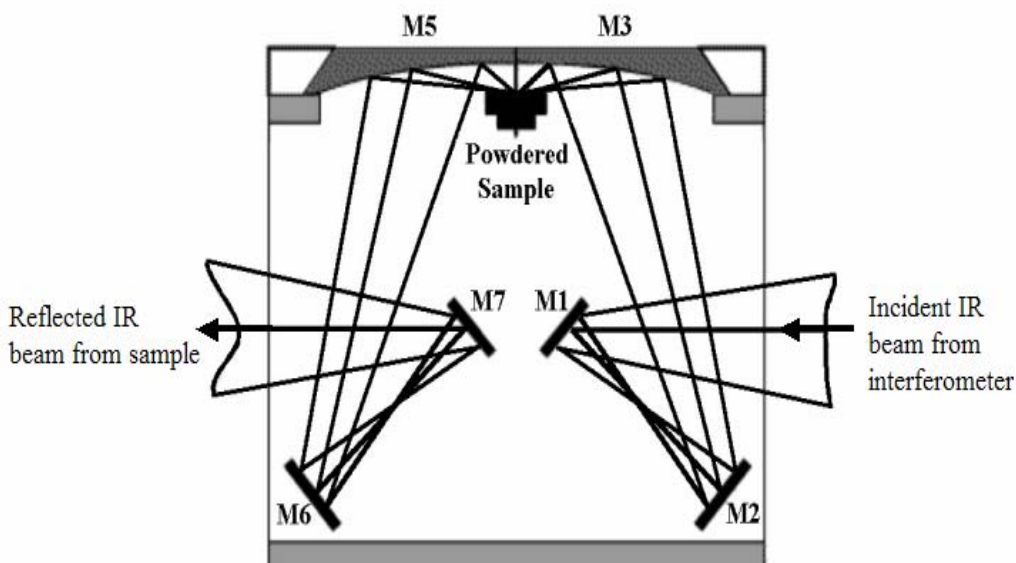


Figure 3: Schematic diagram of the optical arrangement used to measure reflectance spectra in the laboratory.

3.2 Field measurements

A dual-beam interferometer (CATSI) with adjacent fields of view (FOV) was used to perform the passive standoff measurements from radiological materials in the field. The interferometer consisted of a double-pendulum scanning mechanism that controlled the periodic displacement of two corner-cube (CC) reflectors, which generated an interferogram. The beamsplitter consisted of a thin air gap squeezed between two ZnSe substrates having antireflection coatings on their external faces. The output module contained parabolic and

condensing mirrors that focused the beam on a MCT detector (1 mm) mounted on a microcooler. Two CCD cameras mounted on the top of the two telescope modules were used for viewing the scenes under consideration. The symmetrically balanced interferometer provided a differential detection capability in which the two beams of thermal radiation originating from different scenes were optically combined onto the MCT detector and subtracted in real time. Thus, if one beam corresponded to the contaminant-plus-background scene and the other corresponded to only the background scene, then the resulting differential spectrum corresponded primarily to the contaminant target scene. A photograph and an optical diagram of the CATSI instrument are shown in Fig. 4. The standard configuration for the CATSI sensor consisted of two identical Newtonian telescopes, each with a diameter of 10 cm, which were optically coupled to the dual-beam interferometer. Each telescope was capable of being individually aimed at a selected scene, i.e., one on the target scene and the other on a background scene free of the target. This system made it possible to obtain measurements of spectra according to the following specifications: (1) scene FOV of 11 mrad, (2) spectral coverage from 7 to 14 μm , and (3) maximum spectral resolution of 1 cm^{-1} ; however, a resolution of 8 cm^{-1} was used in this work. Coarse and fine adjustments in azimuth and elevation were simply achieved by rotating the whole assembly, which was mounted on a tripod. Additional information on the standard CATSI instrument and its radiometric calibration has been reported elsewhere [10].

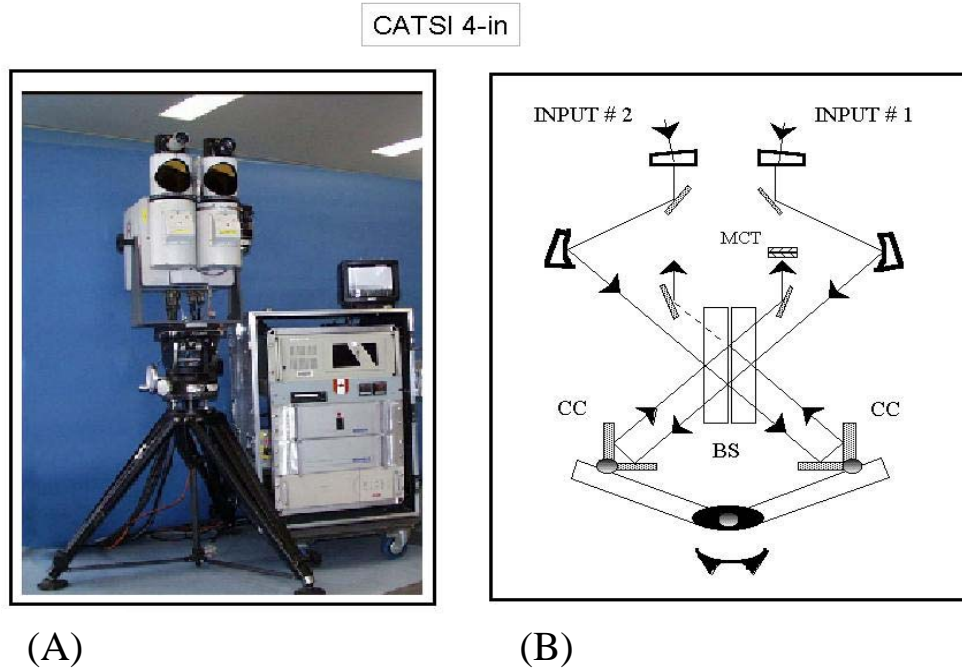


Figure 4: (A) Photograph and (B) optical diagram of the Compact Atmospheric Sounding Interferometer (CATSI) in the standard 10-cm telescope configuration used to passively detect and measure radiological compounds in the field.

4. Results and Analysis

4.1 Laboratory measurements of diffuse reflectance

Examples of the reflectance spectra measured by the DRIFTS technique for UO_2 , UO_3 , U_3O_8 , CoO , Co_2O_3 , IrO_2 , ThO_2 , SrO , I_2O_5 , La_2O_3 and yellow cake are presented in Figs. 5 and 6. The materials exhibit a rich structure throughout the $500\text{--}4000\text{ cm}^{-1}$ ($2.5\text{--}20\text{ }\mu\text{m}$) region and, in particular, within the thermal infrared region of $700\text{--}1400\text{ cm}^{-1}$ ($7\text{--}14\text{ }\mu\text{m}$). The absorption features are attributed to vibrational processes of the solid. Some partial rotation and slight translation can also occur in solids; however, these generate so-called lattice modes that typically occur beyond $20\text{ }\mu\text{m}$ [11]. The absorption features can be very sensitive to small changes in crystal structure or chemistry. In general, the features are much broader than those associated with gases due to the thermal vibrations in the lattice, which have the effect of smearing out the band shape [12].

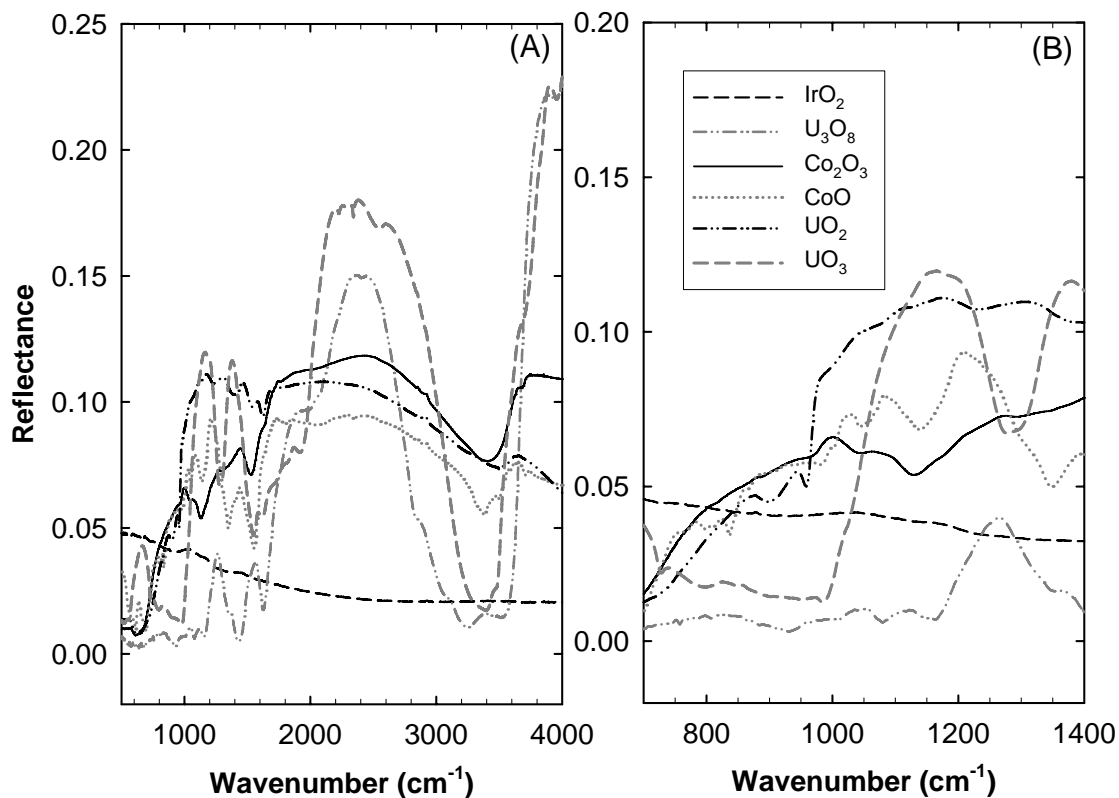


Figure 5: (A) Reflectance spectra measured by the DRIFTS technique for six radiological products over the $500\text{--}4000\text{ cm}^{-1}$ region. The measurements were obtained at a resolution of 4 cm^{-1} . (B) An expanded view of the reflectance spectra over the $700\text{--}1400\text{ cm}^{-1}$ ($7\text{--}14\text{ }\mu\text{m}$) thermal infrared region.

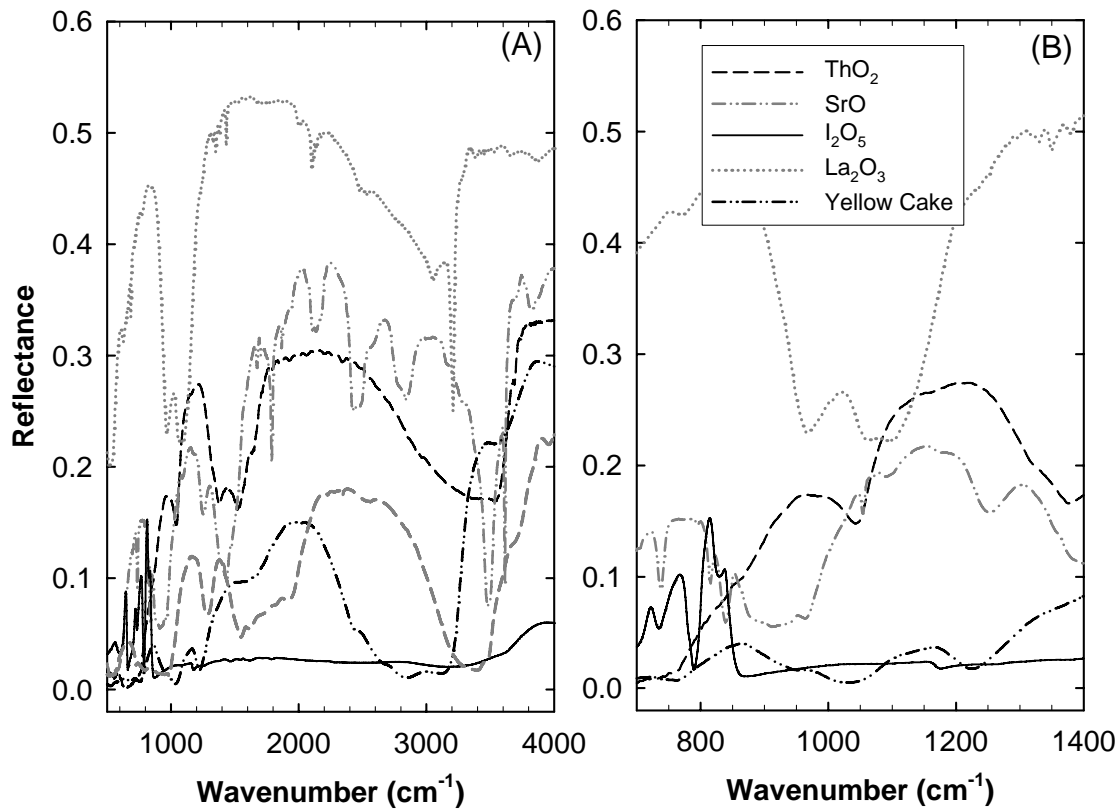


Figure 6: (A) Reflectance spectra measured by the DRIFTS technique for five additional radiological products over the 500–4000 cm^{-1} region. The measurements were obtained at a resolution of 4 cm^{-1} . (B) An expanded view of the reflectance spectra over the 700–1400 cm^{-1} (7–14 μm) thermal infrared region.

4.2 Simulations of the passive standoff detection of radiological materials

To identify a material using a passive standoff detection technique, the energy reflected and emitted by the material at the surface must be transmitted through the atmosphere to the sensor located above at some altitude. Fortunately, the atmosphere is relatively transparent in the 700–1300 cm^{-1} (8–14 μm) region, as shown in Fig. 7 by the transmission spectra of the 1976 U.S. standard atmosphere [13] simulated with the MODTRAN4 model. For a path of 1 m, the atmosphere has an insignificant effect on the radiation emitted or reflected by the surface. This scenario is relevant for the case of a hand-held passive standoff device capable of mapping dispersal patterns of nuclear products on the ground. For longer paths of 0.1–1 km, the atmosphere becomes significantly more opaque, particularly in the spectral range below 700 cm^{-1} and above 1300 cm^{-1} . However, it is apparent that the atmosphere is

sufficiently transmissive in the 750–1250 cm^{-1} region, and this may make it possible to have an airborne passive sensor that is capable of detecting and identifying radiological materials at the surface. For a path of 100 km the typical transmission is about 80%, except in the region of the ozone band near 1000–1100 cm^{-1} , where passive detection may be difficult to achieve.

To summarize, the two main criteria for determining if a passive standoff FTS system has the potential for successfully measuring radiological materials have been achieved: the materials exhibit signatures in the thermal infrared region, and the atmosphere is sufficiently transparent to permit their detection.

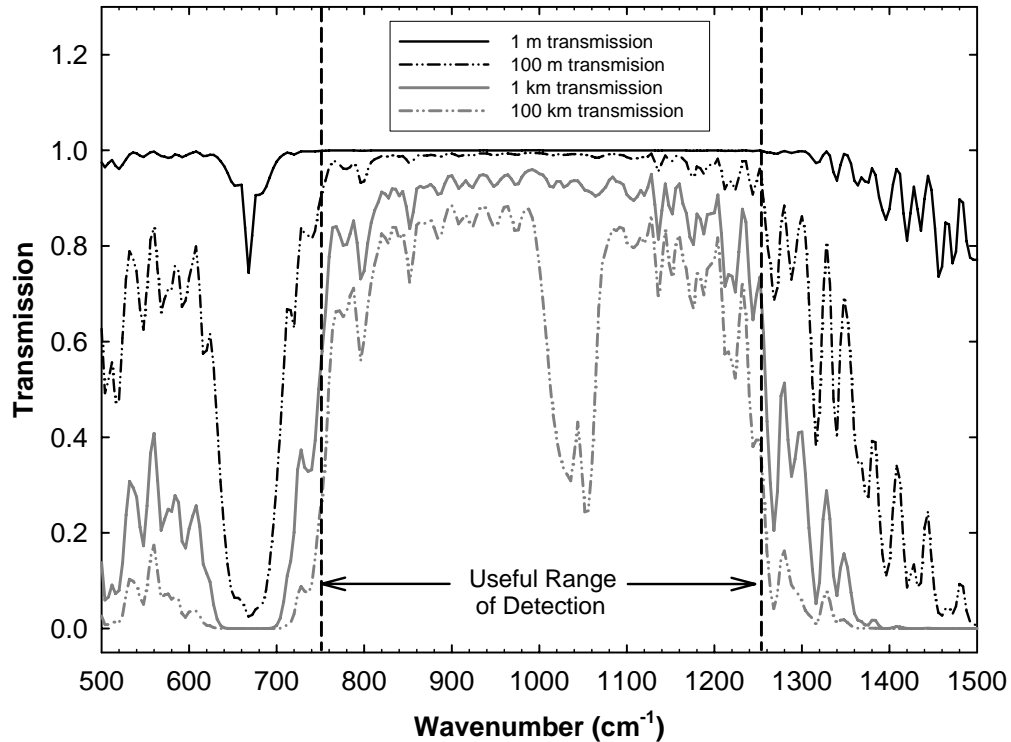


Figure 7: Transmission spectra for different optical depths of the atmosphere as simulated with the MODTRAN4 model.

The MODTRAN4 transmission model was used to simulate the nadir radiance at sensor altitudes of 1 m, 1 km and 100 km above the earth’s surface for several relevant radiological materials including SrO, UO₂, UO₃ and yellow cake. Strontium oxide is of interest in this work since it is the principal radioactive component produced from a RDD consisting of radioactive strontium, which is relatively easy to obtain as a bomb ingredient. The two oxides of uranium are of special interest in the processes related to the nuclear industry, and the detection of yellow cake has potential applicability for uranium mining, particularly in Canada, where the industry is of prime importance. For all simulations, the 1976 U.S. standard atmosphere was used in the MODTRAN4 model, along with the reflectance spectra for the various materials that were measured in the laboratory. It was assumed that the field of view of the sensor was completely filled with the radiological material.

In addition to the direct nadir radiance, simulations of the differential nadir radiance—the difference in radiance between the clean surface and one contaminated with radiological material—were also performed. The differential radiance is minimally affected by atmospheric absorption between the ground and the sensor. In practice it can be readily measured with a dual-beam instrument such as CATSI.

The results of a generic nadir radiance simulation for a sensor altitude of 1 km and a constant surface reflectance of 10% are shown in Figure 8. In this figure, the major contributions to the total radiance are associated with the thermal emission from the surface and the radiance from the atmosphere itself. The reflection of the thermal radiation from the entire sky by the surface has a relatively small contribution, as long as the surface reflectance is not too large, which is usually the case for natural terrains. The effect of the solar radiation is insignificant in the thermal infrared region.

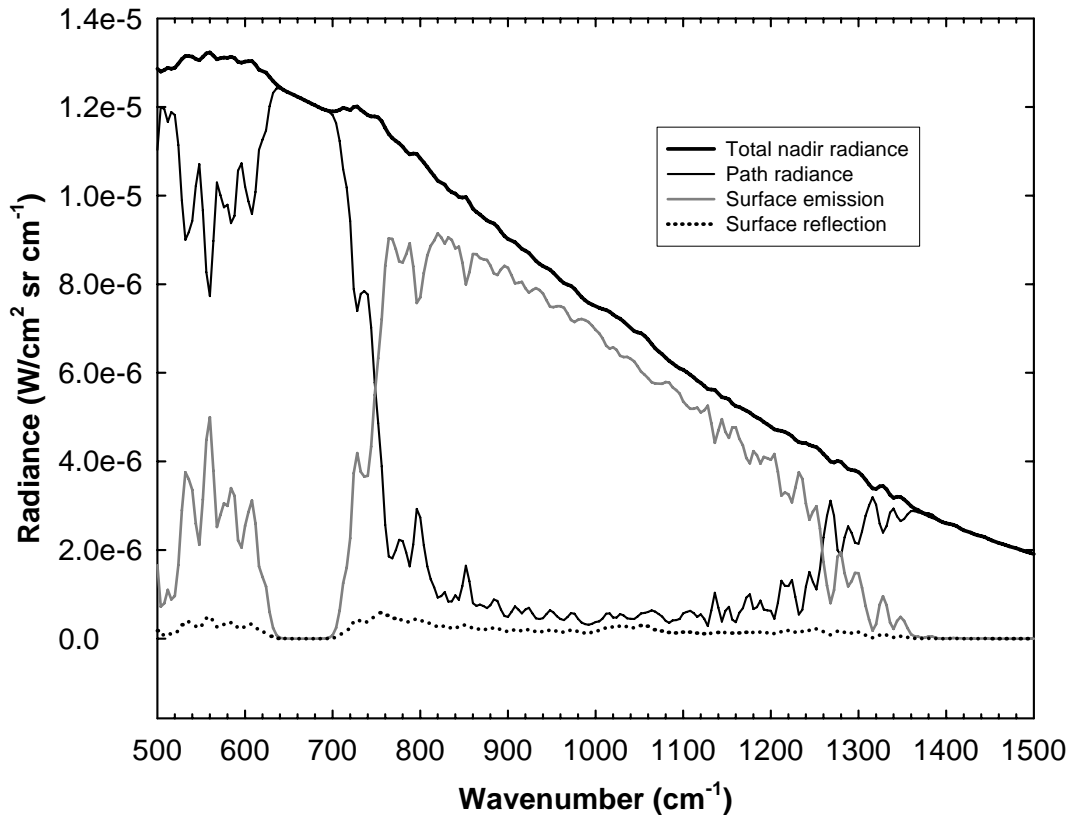


Figure 8: Contributions to total nadir radiance simulated for a sensor at an altitude of 1 km.

4.2.1 Nadir radiance simulations of SrO

The simulated nadir radiance for sensor altitudes of 1 m, 1 km and 100 km and for a surface reflectance based on the laboratory measurement of SrO is shown in Fig. 9. The direct radiances are represented in Fig. 9A along with the Planck radiation for a blackbody at 288.2 K, which represents a non-reflecting surface. For each of the three altitudes, there is a

discrepancy in the 700–1300 cm^{-1} region of the spectrum between the simulated nadir radiance and the blackbody emission that cannot be explained by atmospheric effects. This difference is attributed primarily to the surface reflectance of SrO. The absorption features that are present in the radiance spectra at less than 700 cm^{-1} are associated with carbon dioxide and water vapour, and at greater than 1300 cm^{-1} water vapour is primarily responsible for the absorption. In the nadir simulation for 100 km, the ozone band is present between 1000 and 1100 cm^{-1} . Figure 9B represents the differential radiance simulated with the MODTRAN4 model. The differential radiance represents the difference between two scenes consisting of SrO and a gray body with a reflectance of 15%. In this figure the direct radiance simulated with a gray-body reflectance of 15% was subtracted from the direct radiance simulated for the SrO surface. The dotted curve in Fig. 9B represents the differential radiance spectrum of the SrO without having an atmosphere present. Hence, this curve represents the simulated reference spectrum of the SrO absorption features. It is clear that the simulated differential nadir radiance for all sensor altitudes agrees well with the reference SrO spectrum. The small absorption features that exist throughout the differential spectra are a result of the incomplete cancellation of the reflected atmospheric radiance, which is attributed to differences in the reflectivity of the two surfaces. These simulations suggest that surfaces covered with SrO may potentially be detected with a passive standoff FTS technique.

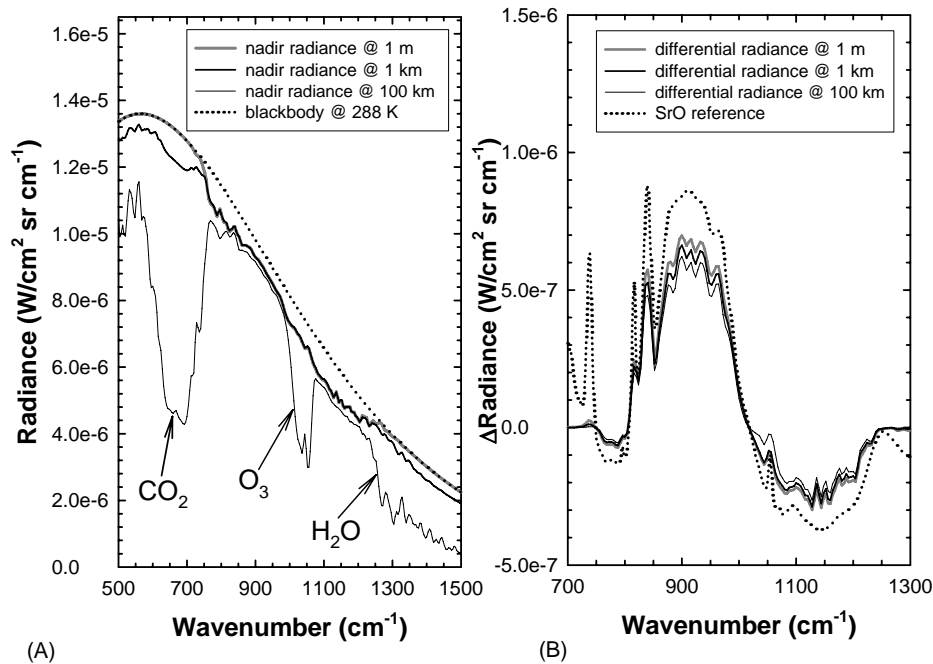


Figure 9: (A) Direct total nadir radiance simulated for three sensor altitudes with a surface consisting of SrO. (B) Differential radiance simulated by subtracting the nadir radiance for a surface with a gray-body reflectance of 15% from the nadir radiance of a SrO surface.

4.2.2 Nadir radiance simulations of UO_2

Figure 10 shows the results from a series of simulations for sensor altitudes of 1 m, 1 km and 100 km using UO_2 for the reflecting surface. Figure 10A represents the direct nadir radiance and Fig. 10B represents the differential radiance. In this case the differential radiance

represents the difference between two scenes consisting of UO_2 and concrete. The radiance simulated for concrete was based on a laboratory measurement of the material's reflectance. The dotted curve in Fig. 10B represents the reference differential spectrum of UO_2 . It was calculated by subtracting the UO_2 radiance from that of a blackbody without having an atmosphere present in order to indicate only those features associated with UO_2 . The presence of UO_2 in the direct nadir spectra of Fig. 10A is not evident; however, the simulated differential nadir radiances in Fig. 10B clearly show the UO_2 feature at 950 cm^{-1} . The differences between the simulated differential spectra and the reference spectrum are attributed to the contribution of the reflected sky radiance, which results from the difference in the reflectance of the UO_2 and concrete backgrounds. The differential radiance spectra deviate significantly from the reference spectrum at $700\text{--}750\text{ cm}^{-1}$. This is attributed to the optically thick CO_2 band, which partially absorbs in this region. Despite the atmospheric interference, the UO_2 signature is clearly identifiable.

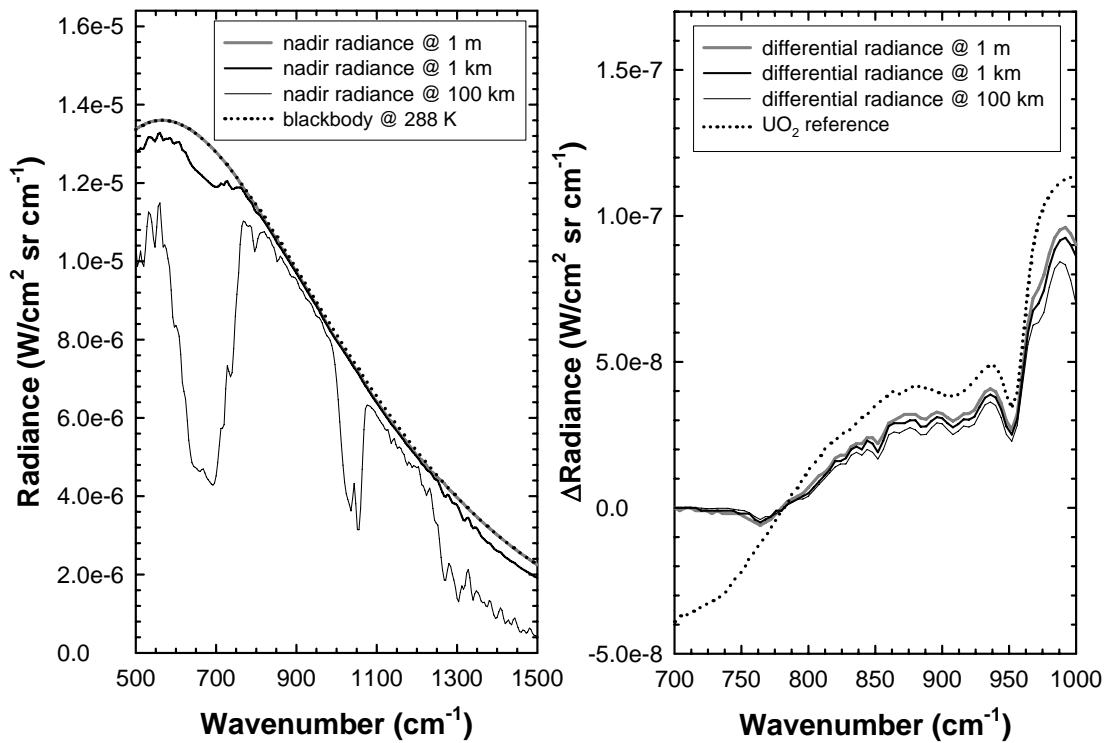


Figure 10: (A) Direct total nadir radiance simulated for three sensor altitudes with a surface consisting of UO_2 . (B) Differential radiance simulation showing the nadir radiance for a concrete surface subtracted from the nadir radiance for a surface of UO_2 . The UO_2 absorption features are clearly visible in the differential spectra.

4.2.3 Nadir radiance simulations of UO_3

Figure 11 shows the results from a similar series of simulations with UO_3 as the reflecting surface. The effect that UO_3 has on the direct nadir radiance is evident near 1100 cm^{-1} in Fig.

11A. Figure 11B represents the differential radiance simulated with the MODTRAN4 model for the three sensor altitudes. In this figure the differential radiance represents the difference in radiance between two scenes consisting of UO_3 and concrete surfaces. The reference differential spectrum of UO_3 was generated in a manner similar to that used in the previous case. There is an obvious discrepancy at $1000\text{--}1100\text{ cm}^{-1}$ between the differential radiance simulated for 100 km and the corresponding radiances for the other altitudes. This is due to the atmospheric ozone band that is present in the spectrum as a result of the differences in the reflectance of the UO_3 and concrete surfaces. Other differences between the differential radiances and the reference spectrum in the $1100\text{--}1300\text{ cm}^{-1}$ region are primarily attributed to water vapour, which does not completely cancel out in the differential mode due to the difference in surface albedo. It is clear that the simulated nadir radiances at 1 m, 1 km and 100 km agree well with the UO_3 reference spectrum, and this suggests that surfaces covered with UO_3 may potentially be identified with a passive standoff FTS technique.

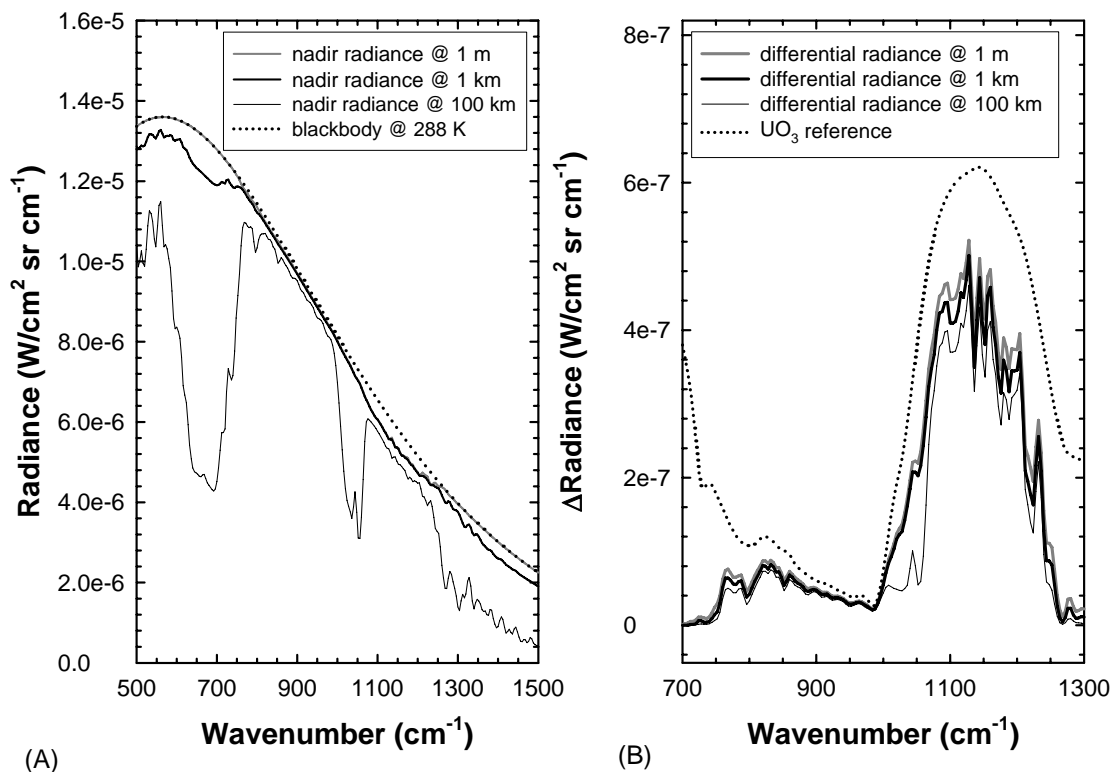


Figure 11: (A) Direct total nadir radiance simulated for three sensor altitudes with a surface consisting of UO_3 . (B) Differential radiance simulation showing the nadir radiance for a concrete surface subtracted from the nadir radiance for a surface of UO_3 . The UO_3 absorption features are clearly visible in the differential spectra.

4.2.4 Nadir radiance simulations of yellow cake

The last material to be considered is yellow cake, a natural uranium ore. For the simulations of the direct radiance from a yellow cake surface, as shown in Figure 12A, the total direct radiance spectra for the three altitudes closely resembles the blackbody curve. This is not

surprising, since in Figure 6B the yellow cake reflection in the transparent window region is only about 2%. Hence, from the simulations of direct radiance, the presence of a yellow cake material covering the surface is not obvious. The situation is improved in the case of the differential simulations shown in Figure 12B, which represent the difference in radiance between two scenes consisting of yellow cake and a gray body with a reflectance of 1%. The latter approximates the reflection from a surface composed of asphalt. Comparison of the differential radiance spectra with the reference spectrum in Fig. 12B clearly shows the presence of the yellow cake bands. It is interesting to note in Fig. 12B that the shape of the absorption feature near 1300 cm^{-1} appears to be shifted to lower energy in comparison with the yellow cake reference spectrum. However, the absorption feature has been reshaped by the optically thick water vapour band, which begins to dominate in this spectral region. It is, therefore, important to base the identification of a compound on the spectral features that are not bordering those of the optically thick atmosphere near 700 and 1300 cm^{-1} .

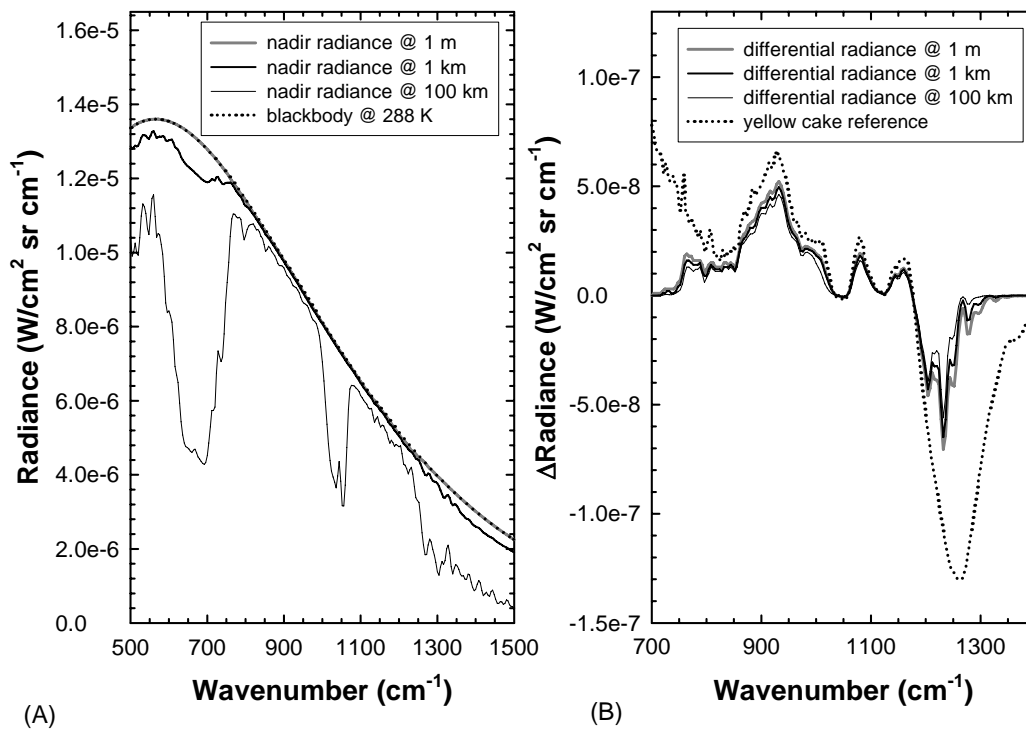


Figure 12: (A) Direct total nadir radiance simulated for three sensor altitudes with a surface consisting of yellow cake. (B) Differential radiance simulated by subtracting the nadir radiance with a gray-body surface reflectance of 1% from the nadir radiance with a yellow cake surface reflectance. The yellow cake absorption features are clearly visible in the differential spectra.

4.3 Effect of temperature contrast on the passive standoff detection of radiological materials

The expression $(B-L_{down})$ in Eq. (4) shows that the intensity of the differential radiance depends on the temperature contrast between the sky and the target on the ground. In order to further examine the effect of the sky temperature on radiance, simulations of the radiance of UO_3 were performed for a number of atmospheric scenarios; clear sky, cloud base at 5 km, cloud base at 1 km and cloud base at 250 m. The optically thick cloud characterizes a blackbody radiating at the temperature of the atmosphere at the altitude where it is located; i.e., clouds located at lower altitudes in the atmosphere are warmer, thereby reducing the temperature contrast with the surface. The simulations of the direct and differential radiance are summarized in Figs. 13A and 13B, respectively. For the case of a cloudless sky where the temperature contrast between the sky and ground is about 80 K in the 700–1300 cm^{-1} region, the differential radiance has a maximum value of about $7 \times 10^{-7} W/(cm^2 sr cm^{-1})$. For an optically thick cloud at an altitude of 5 km, the temperature contrast is reduced to 33 K and the differential radiance decreases by more than a factor of two. In the extreme situation where the cloud is positioned near the ground at an altitude of 250 m, the contrast in temperature is only about 2K and the maximum value of the differential radiance is about $3 \times 10^{-8} W/(cm^2 sr cm^{-1})$. Despite the weak intensity under these conditions, most passive sensors should still have sufficient sensitivity to detect the UO_3 at the surface.

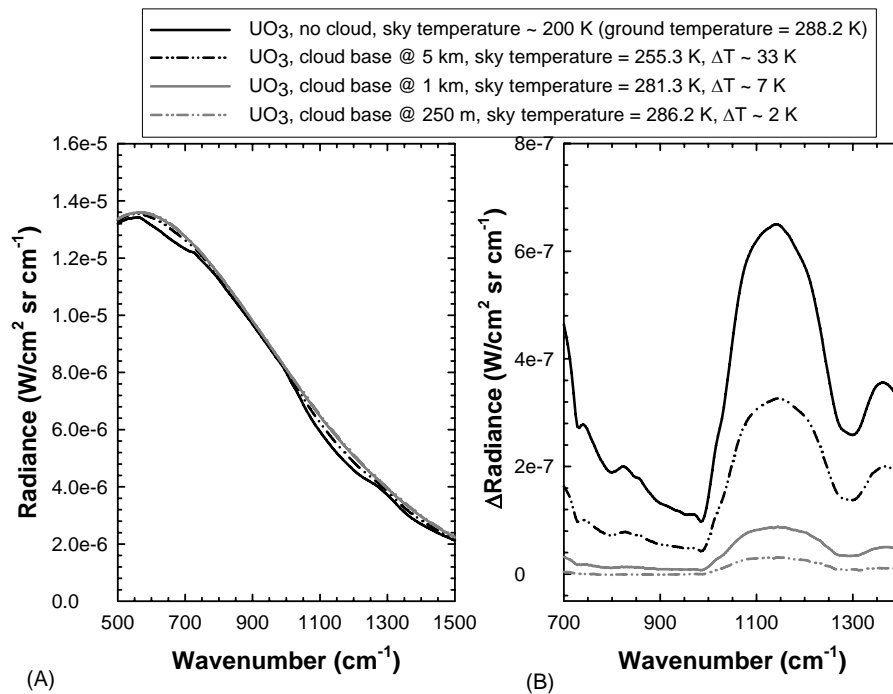


Figure 13: Simulated effect of sky temperature on the passive detection of UO_3 . The sky temperature was altered by changing the base altitude of an optically thick cloud from 5 km to 250 m. (A) Direct total nadir radiance simulated for a surface consisting of UO_3 under varying cloud conditions. (B) Differential radiance simulated by subtracting the radiance of a blackbody at a surface temperature of 288.2 K from the radiance of a surface of UO_3 . The UO_3 absorption features diminish with increased sky temperature.

4.4 Preliminary passive standoff measurements of radiological materials

To further demonstrate the possibility of detecting radiological products passively, a field measurement was performed on 14 October 2003 involving a 5 g powdered sample of SrO sprinkled over an area of 0.2 m² on a stone-tar surface at DRDC Valcartier, as shown in Fig. 14A. The CATSI system was set up at a distance of 10 m from the target, as shown in Figure 14B, and the differential radiance spectrum was measured at a resolution of 8 cm⁻¹ under partly cloudy skies and at a temperature of 20°C. The spectrum, shown in Fig. 15A, consists of the measured difference between the radiance from the SrO powder on the stone-tar surface and from the clean portion of the stone-tar surface adjacent to the powder. Each spectrum consisted of 40 scans, which required a time of 10 s for the measurement. The spectrum is consistent with the differential radiance spectrum simulated for SrO in Fig. 9B. The arrows denote similarities in the SrO features of the measured and reference spectra. The differential radiance spectrum measured in the absence of the SrO powder is also shown to demonstrate the baseline of the differential radiance measurement. A second measurement was performed from a longer standoff distance of 40 m. The resulting differential radiance is presented in Fig. 15B, and, again, there are obvious similarities with the simulated SrO differential radiance reference spectrum.

These two measurements for SrO provide additional evidence for the potential capability of measuring radiological products by non-nuclear methods using passive standoff FTIR radiometry.

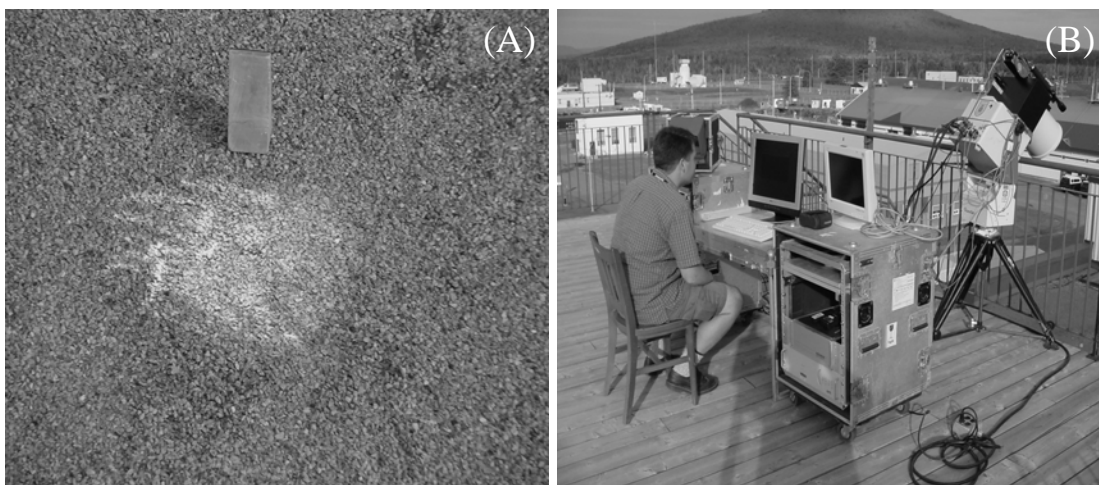


Figure 14: (A) Photograph showing the powdered SrO sample sprinkled on the stone-tar surface. (B) CATSI spectrometer set up to measure the differential radiance of SrO at a standoff distance of 10 m.

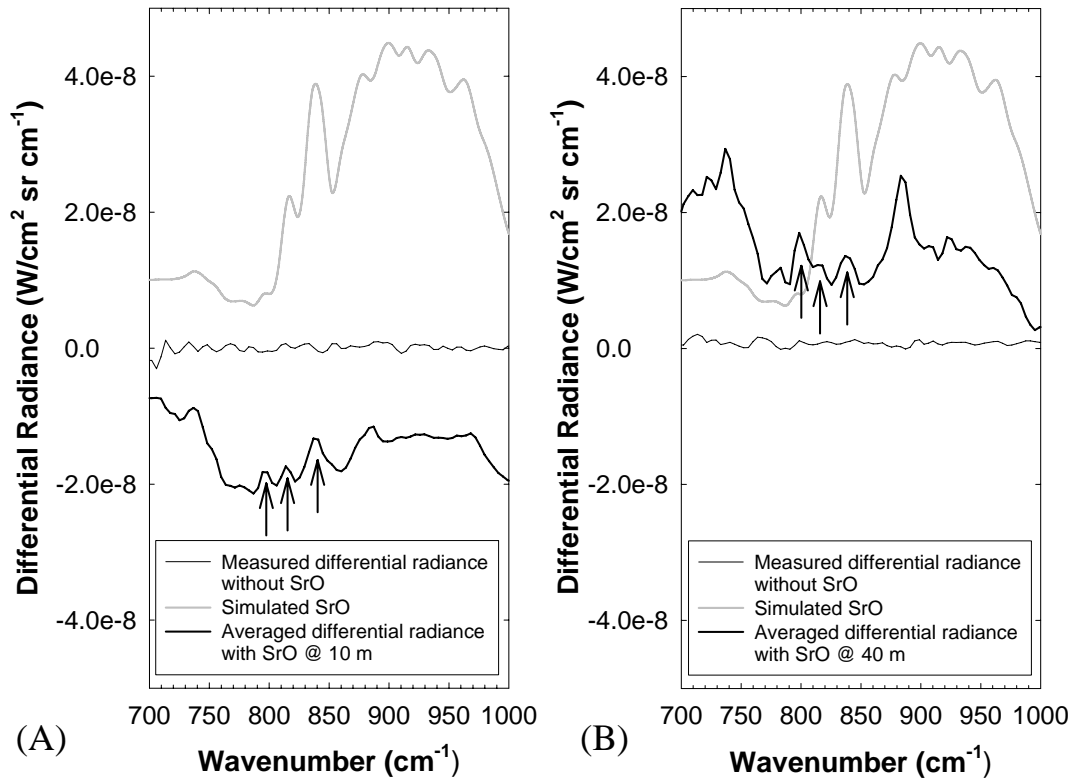


Figure 15: (A) Differential radiance spectra measured at a standoff distance of 10 m for a rooftop contaminated with SrO powder. The simulated differential spectrum of SrO is also presented for comparison. (B) Differential radiance spectra measured at a standoff distance of 40 m.

5. Conclusions

Over the past 18 months, DRDC Valcartier has been investigating the possibility of using passive standoff FTIR radiometry for the detection of radiological materials. The results of this study indicate that a number of strategically important radiological or related materials, including UO_2 , UO_3 , U_3O_8 , CoO , Co_2O_3 , IrO_2 , ThO_2 , SrO , I_2O_5 , La_2O_3 and yellow cake, have detailed infrared signatures in the transparent window region of the thermal infrared spectrum. From a series of simulations performed with the MODTRAN4 model, it has been shown that several of these materials have a potential for being detected and identified in nadir spectra from altitudes of 1 m to 100 km above the earth's surface. These results suggest that radiological materials may be passively detected with compact hand-held FTIR systems or with sensors located on aircraft platforms. The results of the simulations have been reinforced by the results from two field measurements of SrO obtained at standoff distances of 10 to 40 m with the CATSI passive sensor.

This work provides sufficient evidence to warrant further study into the passive detection of radiological products by FTIR radiometric techniques. Future work should include an investigation of mixtures of radiological materials and mixtures of radiological products with non-radioactive materials. A greater range of background surfaces should also be considered for future study, along with the dependence of measurement sensitivity on surface coverage. It would also be of interest to obtain aircraft measurements for altitudes of about 1 km in order to determine experimentally the effectiveness of a passive sensor on an airborne platform.

6. References

1. J.-M. Thériault, E. Puckrin, F. Bouffard and B. Déry, “Passive remote monitoring of chemical vapours by differential FTIR radiometry: results at a range of 1.5 km”, *Applied Optics*, **43**, 1425-1434 (2004).
2. C.T. Chaffin, T.L. Marshall, N.C. Chaffin, “Passive FT-IR remote sensing of smokestack emissions”, *Field Analytical Chemistry and Technology*, **3**, 111-115 (1999).
3. D.F. Flanigan, “Hazardous cloud imaging: a new way of using passive infrared”, *Applied Optics* **36**, 7027-7036 (1997).
4. G. Laufer and A. Ben-David, “Optimized differential absorption radiometer for remote sensing of chemical effluents”, *Applied Optics* **41**, 2263-2273 (2002).
5. J.-M. Thériault, E. Puckrin, J. Hancock, P. Lecavalier, Carmela Jackson Lepage and J.O. Jensen, “Passive standoff detection of chemical warfare agents on surfaces”, *Applied Optics*, **43**, 5870-5885 (2004).
6. J.-M. Thériault and E. Puckrin, “Passive Standoff Detection of BG Aerosol by FTIR Radiometry”, *Applied Optics*, **42**, 6696-6705 (2003).
7. A. Ben-David, “Remote detection of biological aerosols at a distance of 3 km with a passive Fourier transform infrared (FTIR) sensor”, *Optics Express*, **11**, 418-429 (2003).
8. G.P. Anderson, A. Berk, L.S. Bernstein, J.H. Chetwynd, P.K. Acharya, H. Dothe, M.W. Matthew, S.M. Adler-Golden, R.J. Ratkowski, G.W. Felde, J.A. Gardner, M.L. Hoke, S.C. Richtsmeier, B. Pukall, J. Mello, and L.S. Jeong, MODTRAN4: Radiative transfer modeling for remote sensing and atmospheric correction, *Proc., EUROPTO Remote Sensing Congress*, Florence, Italy (1999).
9. D.B. Nash, “Mid-infrared reflectance spectra (2.3–22 μm) of sulfur, gold, KBr, MgO, and halon”, *Applied Optics*, **25**, 2427-2433 (1986).
10. J.-M. Thériault, “Modeling the responsivity and self-emission of a double-beam Fourier-transform infrared interferometer”, *Applied Optics*, **38**, 505-515 (1999).
11. Clark, R. N., Chapter 1: Spectroscopy of Rocks and Minerals, and Principles of Spectroscopy, in *Manual of Remote Sensing, Volume 3, Remote Sensing for the Earth Sciences*, (A.N. Rencz, ed.) John Wiley and Sons, New York, p 3- 58, 1999.
12. B. Hapke, *Theory of reflectance and emittance spectroscopy*, p. 42, Cambridge University Press, Cambridge (1993).
13. G.P. Anderson, S.A. Clough, F.X. Kneizys, J.H. Chetwynd and E.P. Shettle, “AFGL atmospheric constituent profiles (0–120 km)”, AFGL-TR-86-0110 (Air Force Geophysics Laboratory, Hanscom AFB, MA, 1986).

This page intentionally left blank.

Distribution list

INTERNAL

DRDC Valcartier TM 2004-365

- 1 - Director General
- 3 - Document Library
- 1 - J.-M. Thériault (author)
- 1 - E. Puckrin (author)
- 1 - H. Lavoie (author)
- 1 - D. Dubé (author)
- 1 - Hd/SO
- 1 - Hd/GEO
- 1 - Hd/DASO
- 1 - T. Smithson
- 1 - J.-R. Simard
- 1 - M. Lévesque
- 1 - J.-P. Ardouin
- 1 - D. St-Germain
- 1 - L. Bissonnette
- 1 - V. Larochelle
- 1 - G. Roy
- 1 - D. Dion
- 1 - P. Mathieu
- 1 - C. Turcotte
- 1 - J. Lévesque
- 1 - P. Brousseau

EXTERNAL DISTRIBUTION

DRDC Valcartier TM 2004-365

- 1 - DRDKIM (PDF file)
- 1 - DRDC
- 1 - DRDC Ottawa
- 1 - DRDC Atlantic
- 1 - DRDC Suffield
- 1 - DRDC Toronto
- 1 - Director Science and Technology (Command and Control Information Systems)
- 1 - Director Science and Technology (Land)
- 1 - Director Science and Technology (Policy)
- 1 - Director Science and Technology (Maritime)
- 1 - Director Science and Technology (Air)
- 1 - Director Science and Technology (Human Performance)
- 1 - J2 DSI (Directorate Strategic Information)

- 1 - Dr. Tom Cousins
Defence R&D Canada
Radiological Analysis and Defence
3701 Carling Avenue
Ottawa, ON
K1A 0Z4

- 1 - Maj. Rodger Sloan
Director (CTTC) – DRDC Suffield
P. O. Box 4000 Stn Main
Medicine Hat, AB
T1A 8K6

- 1 - Maj. J. F. Legault
DNBCD 2-4
Project Director - Chemical & Radiological Agents
National Defence Headquarters
101 Colonel By Drive,
Ottawa, ON
K1A 0K2

- 2 - Dr. James O. Jensen and Fran D'Amigo
U.S. Army SBCCOM
ATTN: SCBRD-RTE
Building E3549, Room C236
Aberdeen Proving Ground, MD 21010-5423
U.S.A.

DOCUMENT CONTROL DATA

1. ORIGINATOR (name and address) Eldon Puckrin, DRDC Valcartier		2. SECURITY CLASSIFICATION (Including special warning terms if applicable)	
3. TITLE (Its classification should be indicated by the appropriate abbreviation (S, C, R or U) Novel application of FTIR spectroscopy for the passive standoff detection of radiological materials			
4. AUTHORS (Last name, first name, middle initial. If military, show rank, e.g. Doe, Maj. John E.) Puckrin, Eldon. Thériault, Jean-Marc. Lavoie Hugo. Dubé Denis. (DRDC Valcartier)			
5. DATE OF PUBLICATION (month and year) August 2006		6a. NO. OF PAGES 22	6b. NO. OF REFERENCES 13
7. DESCRIPTIVE NOTES (the category of the document, e.g. technical report, technical note or memorandum. Give the inclusive dates when a specific reporting period is covered.) This document is submitted to become a DRDC Valcartier memorandum			
8. SPONSORING ACTIVITY (name and address) DRDC			
9a. PROJECT OR GRANT NO. (Please specify whether project or grant) 0470-1804-71223N		9b. CONTRACT NO.	
10a. ORIGINATOR'S DOCUMENT NUMBER TM2004-365		10b. OTHER DOCUMENT NOS N/A	
11. DOCUMENT AVAILABILITY (any limitations on further dissemination of the document, other than those imposed by security classification) <input checked="" type="checkbox"/> Unlimited distribution <input type="checkbox"/> Contractors in approved countries (specify) <input type="checkbox"/> Canadian contractors (with need-to-know) <input type="checkbox"/> Government (with need-to-know) <input type="checkbox"/> Defense departments <input type="checkbox"/> Other (please specify)			
12. DOCUMENT ANNOUNCEMENT (any limitation to the bibliographic announcement of this document. This will normally correspond to the Document Availability (11). However, where further distribution (beyond the audience specified in 11) is possible, a wider announcement audience may be selected.)			

13. ABSTRACT (a brief and factual summary of the document. It may also appear elsewhere in the body of the document itself. It is highly desirable that the abstract of classified documents be unclassified. Each paragraph of the abstract shall begin with an indication of the security classification of the information in the paragraph (unless the document itself is unclassified) represented as (S), (C), (R), or (U). It is not necessary to include here abstracts in both official languages unless the text is bilingual).

An investigation is made into the possibility of applying the long-wave passive standoff detection technique to the identification of radiological materials. This work is based on laboratory measurements of the diffuse reflectance from a number of radiological or related products, including UO_2 , UO_3 , U_3O_8 , CoO , Co_2O_3 , IrO_2 , ThO_2 , SrO , I_2O_5 , La_2O_3 , and yellow cake. The measured laboratory reflectance signatures were incorporated into the MODTRAN4 radiative transfer model to simulate the nadir radiances of various radiological compounds for three different sensor altitudes. The results of the simulations suggest that passive standoff radiometry may potentially detect and identify radiological materials. Further evidence to support the applicability of the method is based on measurement results from a field trial held at Defence Research and Development Canada – Valcartier involving the passive detection of SrO at standoff distances of 10–40 m.

14. KEYWORDS, DESCRIPTORS or IDENTIFIERS (technically meaningful terms or short phrases that characterize a document and could be helpful in cataloguing the document. They should be selected so that no security classification is required. Identifiers, such as equipment model designation, trade name, military project code name, geographic location may also be included. If possible keywords should be selected from a published thesaurus, e.g. Thesaurus of Engineering and Scientific Terms (TEST) and that thesaurus-identified. If it is not possible to select indexing terms which are Unclassified, the classification of each should be indicated as with the title.)

Passive Standoff Detection, Nuclear, Radiological, Uranium Oxide, FTIR Radiometry

Defence R&D Canada

Canada's Leader in Defence
and National Security
Science and Technology

R & D pour la défense Canada

Chef de file au Canada en matière
de science et de technologie pour
la défense et la sécurité nationale



WWW.drdc-rddc.gc.ca

